First-order melting and dynamics of flux lines in a model for $YBa_2Cu_3O_{7-\delta}$

Seungoh Ryu*
Department of Physics, Ohio State University, Columbus, Ohio 43210

D. Stroud
Department of Applied Physics, Stanford University, Stanford, California 94305
and Department of Physics, Ohio State University, Columbus, Ohio 43210†
(Received 14 February 1996)

We have studied the statics and dynamics of flux lines in a model for $YBa_2Cu_3O_{7-\delta}$, using both Monte Carlo simulations and Langevin dynamics. The lines are assumed to be flexible but unbroken in both the solid and liquid states. For a clean system, both approaches yield the same melting curve, which is found to be weakly first order with a heat of fusion of about $0.02k_BT_m$ per vortex pancake at a field of 50 kG. The time-averaged magnetic field distribution experienced by a fixed spin is found to undergo a qualitative change at freezing, in agreement with NMR and muon spin resonance experiments. The calculations yield, not only the field distribution in both phases, but also an estimate of the measurement time needed to distinguish these distributions: We estimate this time as $\geqslant 0.5$ μsec. The magnetization relaxation time in a clean sample slows dramatically as the temperature approaches the mean-field upper critical field line $H_{c2}(T)$ from below. Melting in the clean system is accompanied by a proliferation of free disclinations and a simultaneous disappearance of hexatic order. Just below melting, the defects show a clear magnetic-field-dependent two- to three-dimensional crossover from long disclination lines parallel to the c axis at low fields, to two-dimensional ''pancake'' disclinations at higher fields. Strong point pins produce an energy varying logarithmically with time. This ln$t$ dependence results from slow annealing out of disclinations in disordered samples. Even without pins, the model gives subdiffusive motion of individual pancakes in the dense liquid phase, with mean-square displacement proportional to $t^{1/2}$ rather than to t as in ordinary diffusion. The calculated melting curve and many dynamical features agree well with experiment. [S0163-1829(96)06626-X]

I. INTRODUCTION

There have been numerous debates about the superconducting-to-normal transition in a magnetic field. Abrikosov's classic mean-field theory predicts a rigid vortex lattice persisting to the mean-field transition line, $H_{c2}(T)$. More recent work suggests that the mean-field Abrikosov transition is altered by fluctuations in both two and three dimensions (2D and 3D). In the 2D case, numerical evidence suggests a first-order melting transition from a vortex solid to a vortex liquid,[1–3] followed at higher temperatures by a gradual crossover to a normal state. In 3D, the suggestion of a first-order fluctuation-induced transition is due to Brézin *et al.*[4] Their argument is based on Landau-level expansion of the Ginzburg-Landau functional for a conventional superconductor.

Much recent work on the 3D flux-lattice melting transition has been stimulated by the behavior of high-T_c materials.[5–7] Several experiments have convincingly demonstrated that the transition there is first order in a sufficiently clean system at sufficiently low fields.[8,9] On the theoretical side, numerical studies of melting have been based on model pairwise interactions,[10–15] the frustrated XY model,[16–18] and an expansion of the free energy in lowest Landau levels (LLL's),[2,3] among other approaches. Some of these calculations[3,17] also indicate that the melting transition in the pure 3D system is first order, as suggested by experiment.

However, numerous issues remain unresolved. One such issue is the effects of disorder on the first-order transition. Disorder is widely expected to modify the first order transition to either a vortex-glass[19] or Bose-glass transition,[20] depending on the type of disorder. Modeling such disorder is difficult because of problems associated with slow relaxation. Much of the modeling has therefore been carried out within the frustrated XY model,[21] a model which introduces an artificial pinning by a fictitious lattice. Other unresolved issues center on the *dynamics* of the solid and liquid vortex system, for which only a very limited number of calculations have been carried out. Dynamical calculations are obviously necessary to understand many measurable properties of the high-T_c materials, such as the I-V characteristics, voltage noise spectra, NMR, and muon spin rotation (μSR). A common approach is to model the high-T_c material as a network of Josephson junctions (a natural dynamical generalization of the frustrated XY model).[22] But as in the static case, this model also suffers from the problem of fictitious pinning, though it is reasonably tractable numerically.

A few dynamical calculations have been carried out using a time-dependent Ginzburg-Landau (TDGL) model within a vortex representation. For example, Enomoto and coworkers have studied various aspects of flux-lattice melting[12] using this approach. They focused on the effects of pin density on the irreversibility line, using as a melting criterion the onset of flux line diffusion. They also considered the transport properties of pinned systems, but studied only configurations consisting of either a single flux line or a two-dimensional lattice with point disorder. Reefman and Brom applied a similar technique to a model for a layered super-

condtor, neglecting the Josephson coupling between layers and focusing on the NMR properties.[14] Most recently, Probert and Rae[15] have performed a Langevin simulation for a model $YBa_2Cu_3O_{7-\delta}$ system, both with and without pins. Their results shed some light on the dynamical distinctions between the irreversibility line (found in disordered systems) and the thermodynamic melting line (characteristic of a clean system). Their calculations, however, assume rigid vortex lines, thereby leaving out some of the most characteristic three-dimensional behavior associated with flexible lines. All these results suggest that this approach may be a useful and quite realistic way to treat the dynamics of flux lines in high-T_c materials.

In this paper, we present a numerical study of both the statics and dynamics of a ''layered London model'' for a three-dimensional flux lattice in $YBa_2Cu_3O_{7-\delta}$, using a combination of Monte Carlo (MC) simulation and Langevin dynamics (LD) within a vortex representation. Our work extends earlier studies in a number of ways. For example, we determine the melting line not only by the motion of individual vortex lines, but also by changes in equilibrium quantities such as the vortex structure factor and a hexatic order parameter. We also determine the conditions under which the vortex lines maintain their integrity, even in the liquid state. Perhaps of greatest interest, we find a 3D-2D crossover in the structure of the vortex solid just below melting, at which the characteristic topological defects change from long disclinations parallel to the c axis to short disclination ''pancakes.'' This crossover may possibly be connected with some recent experimental work, as discussed further below.

The remainder of this paper is organized as follows. The next section describes the model and discusses our choice of parameters suitable for $YBa_2Cu_3O_{7-\delta}$. The following section presents our numerical results as obtained by both Monte Carlo and Langevin simulations. A brief discussion follows in the final section.

II. MODEL

A. Model classical action

In our model, interest is confined to fluctuations in the *phase* degrees of freedom of the superconducting order parameter ψ. The amplitude $|\psi|$ is assumed not to fluctuate, but instead takes the value dictated by minimizing the Ginzburg-Landau free energy at the given temperature T and magnetic induction B. This resulting $|\psi|$ is related to an effective in-plane penetration depth[23] by

$$\lambda_{ab}^2(T,B) \equiv \frac{m^* c^2}{4\pi|\psi|^2 e^{*2}} = \frac{\lambda_{ab}^2(0)}{\{1-[T/T_c(0)]^4\}\{1-[B/B_{c2}(T)]^2\}}, \quad (1)$$

where $T_c(0)$ is the mean-field transition temperature at zero magnetic field, $\lambda_{ab}(0)$ is the in-plane penetration depth at zero temperature, and $B_{c2}(T)$ is the mean-field upper critical field line. $|\psi|$ is normalized so that m^* is twice the electron mass m_e, and $e^*=2e$.

The model consists of N_z parallel superconducting layers a distance d apart. Each layer contains N_v two-dimensional ''vortex pancakes'' (i.e., 2D vortices) described by transverse position coordinates $\mathbf{r}_{i,k}$. The vortex density is assumed to be fixed at $n_B \equiv 1/a_B^2 \equiv B/\phi_0$, where $\phi_0 = hc/2e$ is the flux quantum. Such pancakes in different layers interact via both magnetic and Josephson interactions.[24–27] Here, we simply assume that these interactions combine to produce flexible but *unbreakable* vortex lines — that is, each pancake is always associated with two specific pancakes in the adjacent layers. The justification and possible limitations of this assumption are discussed below. The interlayer coupling strength is characterized by a single variable $\gamma = \xi_{ab}(0)/\xi_c(0)$, where $\xi_{ab}(0)$ and $\xi_c(0)$ are the zero-temperature superconducting coherence lengths in the ab plane and c direction. γ has associated with it a length scale $r_g \equiv \gamma d$. The layered structure becomes important for lengths shorter than r_g.[28]

Following Ref. 11, we write down the Hamiltonian for the system as

$$\mathcal{H} = \sum_{i\neq j}\sum_k U\left(\frac{|\mathbf{r}_{i,k}-\mathbf{r}_{j,k}|}{\lambda_{ab}(T,B)}\right) + \sum_i \sum_k V\left(\frac{|\mathbf{r}_{i,k}-\mathbf{r}_{j,k}|}{2r_g}\right). \quad (2)$$

Here the in-plane repulsive interaction takes the form

$$U(x) = \frac{d\phi_0^2}{8\pi^2\lambda_{ab}(T,B)^2} K_0^*(x), \quad (3)$$

while the interlayer interaction is taken as

$$V(x) = c_J(x-1) \quad (x>1),$$
$$= c_J(x^2-1) \quad (x\leq 1), \quad (4)$$

with

$$c_J = \frac{d\phi_0^2}{8\pi^3\lambda_{ab}(T,B)^2}\left[1+\ln\frac{\lambda_{ab}(0)}{d}\right]. \quad (5)$$

In order to reduce finite-size effects, we employ periodic boundary conditions in all directions. Because of these, the effective in-plane interaction becomes $K_0^*(x)$, which represents the summation of the modified Bessel function $K_0(x)$ over image vortices.[29]

B. Langevin dynamics

To probe real time dynamics, one can also run LD simulations on the same model, assuming that the vortices are subject to an overdamped dynamics. Then the equation of motion for a vortex pancake can be written

$$\eta\dot{\mathbf{r}}_{i,k}(t) = \mathbf{f}_{i,k}^T(t) + \mathbf{f}_{i,k}^U(t) + \mathbf{f}^L + \mathbf{f}^P(\mathbf{r}_{i,k}). \quad (6)$$

The first term on the right-hand side is the Brownian force due to thermal noise. The noise is assumed to be Gaussian-distributed white noise with correlation functions

$$\langle f_{i,k}^T(t)\rangle = 0, \quad (7)$$

$$\langle[\mathbf{f}_{i,k}^T(t)\cdot\hat{n}_\alpha][\mathbf{f}_{j,k'}^T(t')\cdot\hat{n}_\beta]\rangle = 2k_BT\frac{\eta}{d}\delta_{ij}\delta_{\alpha,\beta}\delta_{kk'}\delta(t-t'), \quad (8)$$

where $\hat{n}_\alpha$ is a unit vector in the α direction, $\alpha=x,y$. The second term on the right-hand side of Eq. (6) is the force due to the other pancakes; it is obtained as a negative spatial gradient of the vortex-vortex interaction term, as written down in Eqs. (3) and (4). The third term (not studied numerically in the present paper) is the Lorentz force due to an applied current.

The last term in (6) describes the force due to the random pinning potential. The pins are modeled as uniformly cylindrical regions of radius r_p [taken to be $2\xi_{ab}(0)$ throughout this work]. The pinning energy of the vortex pancake is expected to be determined by the fraction of the core area within the pinning well. We can achieve this dependence by assuming a pinning energy per pancake, $U_p(T,B)=\alpha_p d\phi_0^2/[16\pi^2\lambda_{ab}^2(T,B)]$. Thus, the strength of a single pin is controlled by the dimensionless parameter α_p. The effectiveness of the pins is, of course, also influenced by their areal density n_p or the ''equivalent field'' $B_p\equiv\phi_0 n_p$.

For simplicity, the force due to the lth point pin is assumed to be directed radially inward towards its center (at $\mathbf{R}_l$). For $r_p>\xi_{ab}(T)$ it is given by

$$f_l^P(\mathbf{r}_{i,k})=\begin{cases} -\dfrac{U_p(T,B)}{2\xi_{ab}(T)} & \text{if } r_p-\xi_{ab}(T)<|\mathbf{r}_{i,k}-\mathbf{R}_l|<r_p+\xi_{ab}(T), \\ 0 \quad \text{otherwise.} \end{cases} \tag{9}$$

For $r_p<\xi_{ab}(T)$, it takes the form

$$f_l^P(\mathbf{r}_{i,k})=\begin{cases} -\dfrac{U_p(T,B)}{r_p+\xi_{ab}(T)}\left(\dfrac{r_p}{\xi_{ab}(T)}\right)^2 & \text{if } 0<|\mathbf{r}_{i,k}-\mathbf{R}_l|<r_p+\xi_{ab}(T), \\ 0 \quad \text{otherwise.} \end{cases} \tag{10}$$

This choice includes in the simplest manner the fact that the vortex core area grows with increasing T while the disorder is temperature independent.

C. Numerical approach and choice of parameters

To obtain the thermodynamics via MC simulation, we use the standard Metropolis algorithm with variable step sizes, as discussed in Ref. 11. Typically, we equilibrate over 2×10^4 MC steps and evaluate the thermodynamic averages over an additional $2\times10^4-10^5$ steps.

For both MC and Langevin calculations, we use lookup tables for both the potential and the forces, as well as a scheme for interpolating between the points in the table. The time iteration is carried out using a second-order Runge-Kutta algorithm in time steps of Δt_0 where

$$t_0=\frac{\phi_0}{B}\frac{d\eta}{(32)^2\epsilon_d}$$

and

$$\epsilon_d=\frac{d\phi_0^2}{8\pi^2\lambda_{ab}(0)^2}.$$

The choice of Δ is dictated by the dominant forces in our model [Eq. (6)], which in this paper are the vortex-vortex interactions; in general, $\Delta\leq O(10)$. For optimum convergence, we have allowed Δ to depend somewhat on T, B, and J, since different components of the force may dominate at different values of these parameters.

Finally, we briefly discuss our choice of parameters. For $\lambda_{ab}(0)$, we use 1000 Å for $YBa_2Cu_3O_{7-\delta}$ single crystal. This choice is close to the experimentally determined value, and also places the simulated melting curve in close agreement with the experimental data of Ref. 8. For the remaining parameters, we use the values appropriate for $YBa_2Cu_3O_{7-\delta}$: $\kappa=87.5$, $d=11.1$ Å, $\gamma=5$, $T_c(0)=93$ K, and $dH_{c2}(T)/dT=-1.8\times10^4$ Oe/K, where $\kappa\equiv\lambda_{ab}(0)/\xi_{ab}(0)$ is the Ginzburg-Landau parameter.

D. Calculated quantities

Before discussing our numerical results, we first define a few important physical quantities. $\delta R(t)$ is the transverse root-mean-square (rms) displacement of a pancake vortex from its average position, i.e.,

$$\delta R(t)\equiv\frac{1}{a_B}\left\{\frac{1}{N_{\rm tot}}\sum_{i,k}\langle(\mathbf{r}_{i,k}-\langle\mathbf{r}_{i,k}\rangle_t)^2\rangle_t^{1/2}\right\}. \tag{11}$$

Here $\langle\cdots\rangle_t$ denotes an average over time t, and $N_{\rm tot}=N_zN_v$ is the total number of pancakes. Now in a finite system, as in our simulation, the collection of vortex lines tends to drift as a whole even in the solid phase. This behavior, seen in both solid and liquid phases, is strictly a finite-size effect and has no relation to any measurable quantities. We therefore subtract out the drift by using $\mathbf{r}_{i,k}^*(t)=\mathbf{r}_{i,k}(t)-\mathbf{R}_{\rm c.m.}(t)$ instead of $\mathbf{r}_{i,k}$ in Eq. (11), $\mathbf{R}_{\rm c.m.}(t)$ being the instantaneous center-of-mass coordinate of the entire lattice. To monitor lateral fluctuations, we also calculate the ''wandering length'' l_T (Ref. 30) defined by

$$l_T^2\equiv\frac{1}{N_{\rm tot}a_B^2}\sum_{i,k}\langle|\mathbf{r}_{i,k}-\mathbf{r}_{i,k+1}|^2\rangle_t. \tag{12}$$

In addition, we compute the density-density correlation function

$$C(\mathbf{r},z)=\langle\rho_v(\mathbf{r},z)\rho_v(\mathbf{0},0)\rangle_{t\to\infty} \tag{13}$$

and its partial Fourier transform

$$S(\mathbf{q},z)=\int d^2rC(\mathbf{r},z)\exp(i\mathbf{q}\cdot\mathbf{r}), \tag{14}$$

where $\rho_v(\mathbf{r},z)$ is the local vortex number density in each plane z and $\mathbf{q}=(q_x,q_y)$.

III. NUMERICAL RESULTS

A. Location of melting curve: heat of fusion

To locate the melting point for a given B by MC simulation, we first make a quick sweep over a wide range of temperatures ($\sim$20 K), using 2×10^4 MC steps for each T in steps of $\Delta T\sim0.5$–1 K. We interpret a discontinuous jump in $\delta R(t)$ as well as the vanishing of the intensity of the Bragg peak $S(\mathbf{q},0)$ at $\mathbf{q}=\mathbf{G}_2$ (where $\mathbf{G}_2$ is a 2D reciprocal lattice vector of the triangular lattice) as signatures of melting. We then repeat more careful sweeps over a narrower temperature region with up to 10^5 MC steps.

If the temperature is cycled through T_m using an interval of 10^4–3×10^4 MC steps for each temperature in increments $\Delta T/T_m=0.0024$, we observe hysteresis in most monitored quantities. The width of the loop is typically $\approx0.018T_m$. Hysteresis is most pronounced for $\delta R(t)$ and for the disclination density (defined below), but is also quite conspicuous for the hexatic order parameter (also defined below) in the same temperature range. From the size of the jump in the total internal energy seen at melting, we estimate the latent heat per vortex pancake to be about $0.034\pm0.01k_BT_m$. (A possibly more precise estimate is given below.) The melting transition is calculated to occur at $T_m(B)/T_{c2}(B)=0.87\pm0.02$, 0.93 ± 0.006, and 0.93 ± 0.02, for $B=90$, 50, and 10 kG respectively, and lattices with eight layers, in reasonable accord with experiment.[8] For lattices with 32 layers and $\lambda_{ab}=1400$ Å, we obtain $T_m(B)/T_{c2}(B)=0.86\pm0.02$, 0.92 ± 0.02, and 0.96 ± 0.02 at the same fields. [Here $T_{c2}(B)$ is the mean-field transition temperature at field B.] Since our assumed T dependence of $\lambda_{ab}(T,B)$ is likely to become less accurate as $T\rightarrow T_c(0)$, we may expect increasing deviations from experiment at lower fields, as indeed we find in our calculations. Note that, for the higher fields, $T_m/T_{c2}(B)$ depends little on either the lattice aspect ratio or the value of λ_{ab}. This behavior is consistent with the dimensional crossover discussed below.

The transverse displacement $\delta R(t)$, as expected, shows characteristically different behavior in the solid and liquid phases. In the liquid, $\delta R(t)$ increases with increasing t (see below), while in the solid phase, it saturates after a short transient period. The inset to Fig. 1 shows the behavior of $\delta R(t)$ across the melting transition for $B=50$ kG, as calculated by MC simulation. Also shown are the Langevin results, which agree very well with MC predictions. This confirms that the two indeed give, as expected, very similar predictions for thermodynamic quantities. From the results in the solid phase, we can read off the Lindemann number $c_L\equiv\delta R(T_m,B)=0.18$, at $B=50$ kG. We have not, however, confirmed that c_L is constant along the melting curve, as would be expected if Lindemann's law is really valid.

Another way to display the first-order melting process is also shown in Fig. 1. The MC energy at any given temperature fluctuates with MC time. The two curves in the main part of Fig. 1 show the distributions of total internal energy within two different time windows at the melting temperature [(a) and (b) in Figs. 1 and 2]. On either side of T_m, this distribution tends to be independent of the initial time of the window. Precisely at T_m, however, the system slowly oscillates between a liquid and a solid phase with a correlation time of about 5×10^4 MC time steps (for this system size). The oscillation causes the two distributions to differ: The two distributions shown are the extreme cases that we have found in the length of time studied. As shown in the insets at the bottom of Fig. 2, the density correlation functions in the ''low-energy'' and ''high-energy'' windows do indeed show solidlike and liquidlike characteristics. We believe that the weak hexagonal symmetry seemingly present in the ''liquid'' phase actually results from the presence of a few solid configurations in the window, and possibly also from the finite size of the sample.

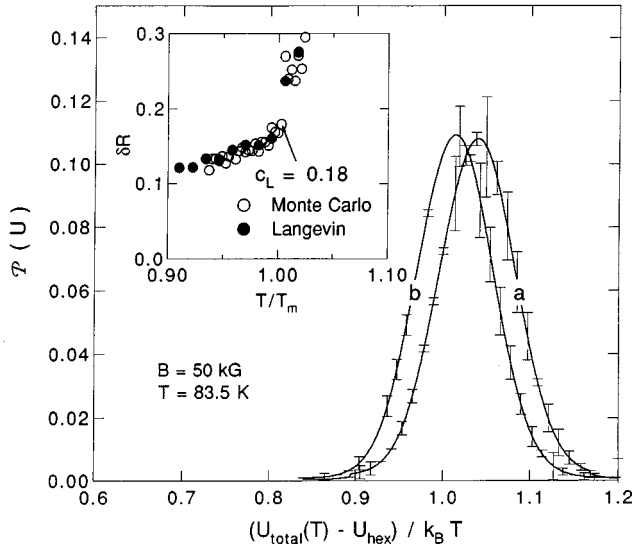

FIG. 1. Probability distribution $\mathcal{P}(U)$ for the total internal energy $U_{\rm total}(T)$ per pancake, averaged over two different time windows (a) and (b) (specified in Fig. 2), at the melting temperature T_m. Calculation is carried out for $YBa_2Cu_3O_{7-\delta}$ at $B=50$ kG. $U_{\rm hex}$ is the corresponding energy for a perfect triangular lattice of straight vortex lines (the minimum energy configuration). The distributions in each window are obtained by dividing the data from the Monte Carlo configurations shown in Fig. 2 into 256 energy bins, each of width $\triangle U/k_BT=1.4\times10^{-4}$. The curves are least-squares fits of these data to Gaussian distributions. The error bars at various values of $U_{\rm total}$ are the rms deviations of the values of $\mathcal{P}(U)$ inferred from ten bins in the vicinity of U. Inset: in-plane rms displacement c_L of pancake vortices from their equilibrium lattice positions in units of lattice spacing, as calculated using both Monte Carlo and Langevin techniques.

From the average energy difference between the two phases as read from Fig. 2, and also from the distance between the peaks in Fig. 1, we estimate the heat of melting to be $\lesssim0.02k_BT_m$ per vortex pancake. This estimate for the heat of fusion is in agreement with LLL calculation of Ref. 3, as well as with experimental estimates at high fields. It is significantly smaller, however, than the value of Hetzel *et al.*[17] of $0.3k_BT_m$ per vortex pancake, obtained using a frustrated

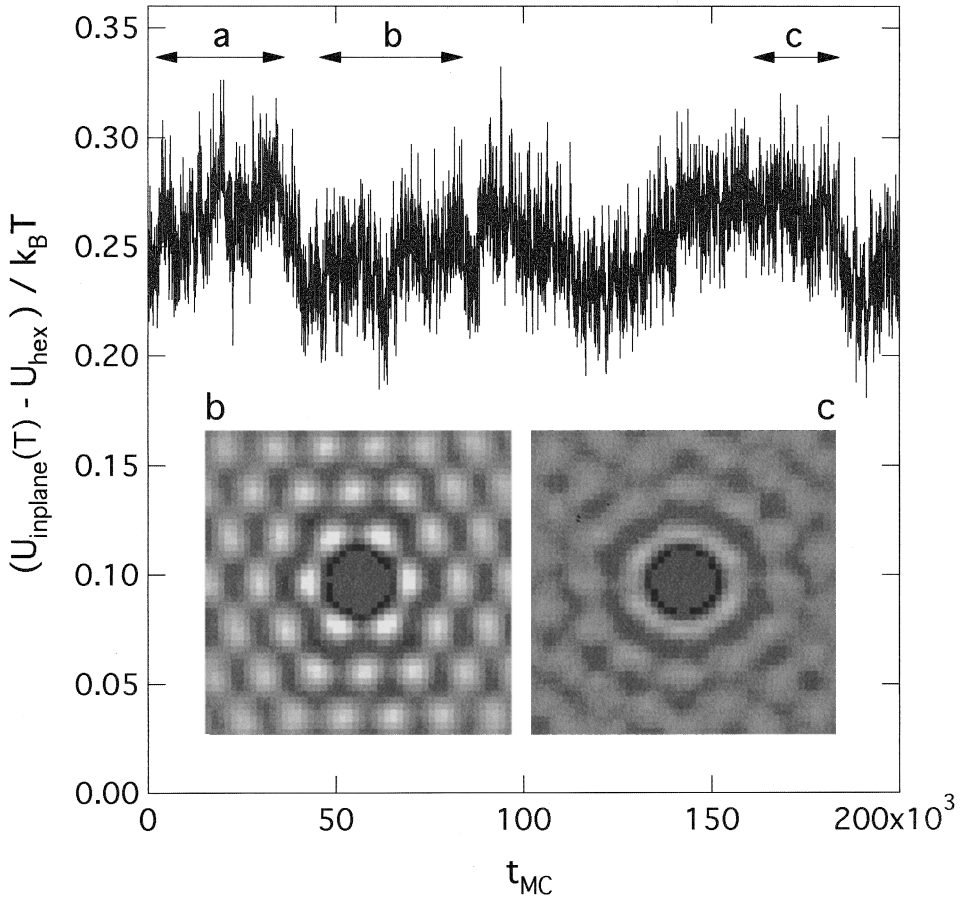

FIG. 2. Evolution of the in-plane component of internal energy, $U_{\text{in plane}}(T)$, at the melting temperature, for $B=50$ kG as calculated via MC simulation. Insets: density-density correlation $C(\mathbf{r},0)$, averaged over the two different time windows (b) and (c). These plots show that the system is alternating between lattice and liquid phases.

stacked triangular XY model. The reasons for this difference are a matter of speculation. One possibility is that in both our simulations and the LLL model, $|\psi|$, which sets the overall energy scale, decreases with increasing temperature, whereas in the XY simulation, the coupling strength J is temperature independent. More plausibly, our simulations are carried out at high fields while the XY simulations are more appropriate at low fields. Yet a third (unlikely) possibility is that our simulations allow for anisotropy in the superconducting properties, whereas those of Hetzel *et al.* do not.

We find that most of the energy discontinuity at melting comes from changes in the interaction energy between different pancakes in the same layer, which has a rather clear jump at melting. By contrast, the interlayer coupling energy has large fluctuations in both the solid and liquid phases but no clear jump. These fluctuations tend to mask the steplike change of the in-plane component.

B. Topological defects in clean $YBa_2Cu_3O_{7-\delta}$

We have carried out a search for topological defects above and below melting in our model for $YBa_2Cu_3O_{7-\delta}$. Basic building blocks for various kinds of topological defects are disclinations and dislocations. Both kinds of defects may be identified by carrying out a Delaunay triangulation[31] for individual layers of each sampled configuration. To understand this procedure, we show in Fig. 3 a snapshot of a typical melted configuration in a single layer which shows both *bond lines*, as identified by the Delaunay procedure, and *topological defects*. The vortex pancakes are located at the vertices of the triangles. They are marked by black and grey dots if their number $n(i)$ of in-plane neighbors is 7 (positive disclination) or 5 (negative disclination) rather than the 6 expected for a perfect triangular lattice. We see characteristic examples of an isolated dislocation [i.e., a pair of disclinations, marked by (a)], an isolated disclination (b), and a bound pair of dislocations (c). In the present work, we arbitrarily call a pair of disclinations ''bound'' if and only if they reside on neighboring pancakes as in (a) and (c).

For a more quantitative analysis of the defect configurations, we assign ''charges'' $q(i,z)=n(i,z)-6$ to the izth pancake, where $n(i,z)$ is the number of in-plane neighbors of the izth pancake. The *average* total defect density is defined by

$$n_d=\frac{1}{N_v N_z}\sum_{i,z} n_q(i,z),$$

where $n_q(i,z)=1-\delta_{q(i,z),0}$. (Note that this definition includes defects of both signs.) Since tightly bound neutral pairs of disclinations, such as (a) and (c), do not influence local hexatic order (i.e., the degree of local sixfold symmetry), it is also useful to define an *isolated* charge density by

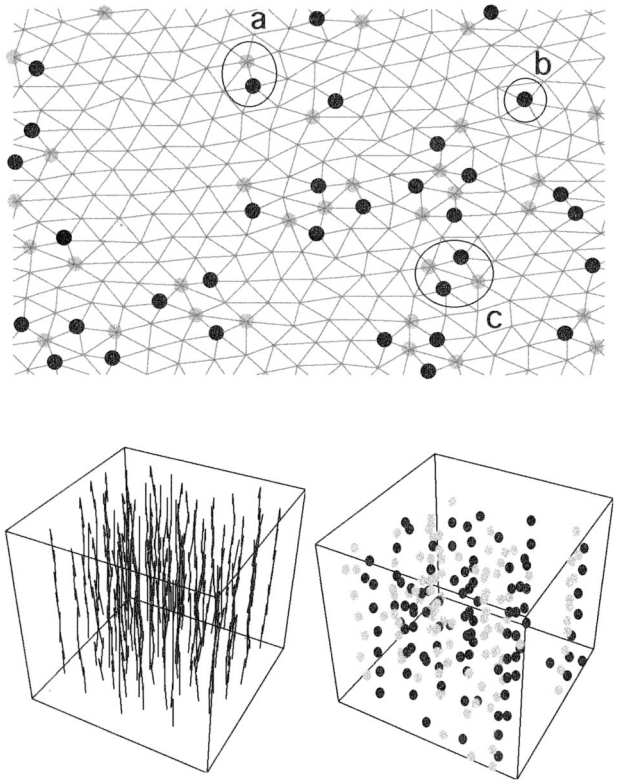

FIG. 3. Snapshot of disclination distribution in a single layer of a vortex liquid containing 256 lines, as determined by Delaunay triangulation. Black dots, fivefold disclinations; gray dots, sevenfold disclinations. (a) A pair of bound disclinations, equivalent to a dislocation; (b) an isolated disclination; (c) a pair of bound dislocations. The bottom row shows a typical vortex line liquid and its representation in terms of disclinations of either sign.

$q^*(i,z)=q(i,z)+\Sigma_j' q(j,z)$, where the prime indicates that j runs over the in-plane neighbors of pancake (i,z). This definition eliminates bound-pair defects such as (a) and (c). The *average* isolated charge density is then defined by

$$n_d^*=\frac{1}{N_v N_z}\sum_{i,z} n_q^*(i,z),$$

where $n_q^*(i,z)=(1-\delta_{q^*(i,z),0})$.

Once the charges are identified on each plane, the topological defect configuration associated with a given vortex arrangement (lower left in Fig. 3) may be represented as a ''neutral plasma'' of line charges of variable lengths l_d and both signs (cf. Fig. 3, lower right). To quantify the properties of this plasma, in our simulation, we monitor the distribution of defect lengths of either sign $\mathcal{P}(l_d)$, defined as

$$\mathcal{P}(l_d)=\frac{1}{N_z N_v}\left\langle \sum_{i,z}\sum_{q}[1-n_q(i,z_0)] \times[1-n_q(i,z_0+l_d+1)]\prod_{z=z_0+1}^{z_0+l} n_q(i,z)\right\rangle_t . \tag{15}$$

We also monitor the in-plane hexatic order parameter Ψ_6, defined by

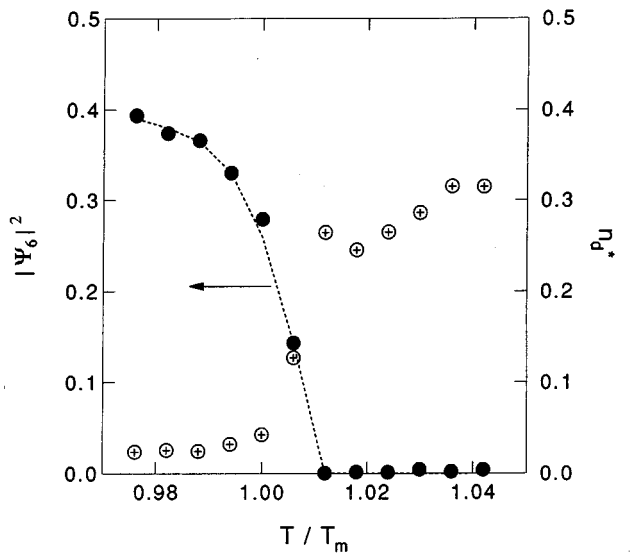

FIG. 4. Hexatic order parameter $|\psi_6|^2$ (left scale) and density of isolated disclinations n_d^* (right scale) as a function of temperature in a 64-line system of thickness 8 layers with $B=50$ kG.

$$\Psi_6=\frac{1}{N_v N_z}\sum_{i,z}\frac{1}{n(i,z)}\sum_j \langle\exp[6i\theta_{ij}(z)]\rangle, \tag{16}$$

where $\theta_{ij}(z)$ is angle made by the bond between vortices i and j and the x axis. The results are shown in Fig. 4. Evidently, melting is accompanied by a proliferation of isolated dislocation and disclination lines, as well as by a dramatic drop in the in-plane hexatic order parameter. Near T_m, but still below it, transient line defects are observed to appear and disappear, while at T_m there is an abrupt decrease in hexatic order accompanied by an almost discontinuous jump in n_d^* (cf. Fig. 4). $|\Psi_6|$ appears to vanish no more than 1% above T_m. While we cannot rule out a ''hexatic line phase'' (with hexatic but no long-range crystalline order) within this temperature range, our numerical results are consistent with a single melting transition where both hexatic and crystalline order simultaneously disappear.

As the flux line density increases, the interlayer coupling becomes weaker compared to the in-plane interaction. Hence, one might expect a dimensional crossover in the defects associated with the melting transition. Indeed, we find such a crossover in the solid phase. In Fig. 5, we show the length distribution $\mathcal{P}(l_d)$ for 32 layers at several fields ($B=10$, 50, 90 kG) and temperatures slightly below T_m ($T/T_m=0.997$, 0.982, 0.988) selected with the criterion of $\delta R=0.15$ for consistency. In each case, by monitoring $C(\mathbf{r},z)$ and $S(\mathbf{q},z)$, we verified that the system is solid, but very near melting. As evidence that the lattice anisotropy depends on field, we note that for the same value of in-plane rms fluctuations ($\delta R=0.15$), l_T is field dependent: At fields of 10, 50, and 90 kG, it is respectively 0.077, 0.100, 0.114.

The topological defects *have a dramatic crossover* as a function of field. This is obvious from the right-hand column of the figure. At the lowest field (10 kG), there are line defects penetrating all the way through the sample, which occur only for temperatures extremely close to melting ($T/T_m>0.99$). At higher fields, the defect line segments are

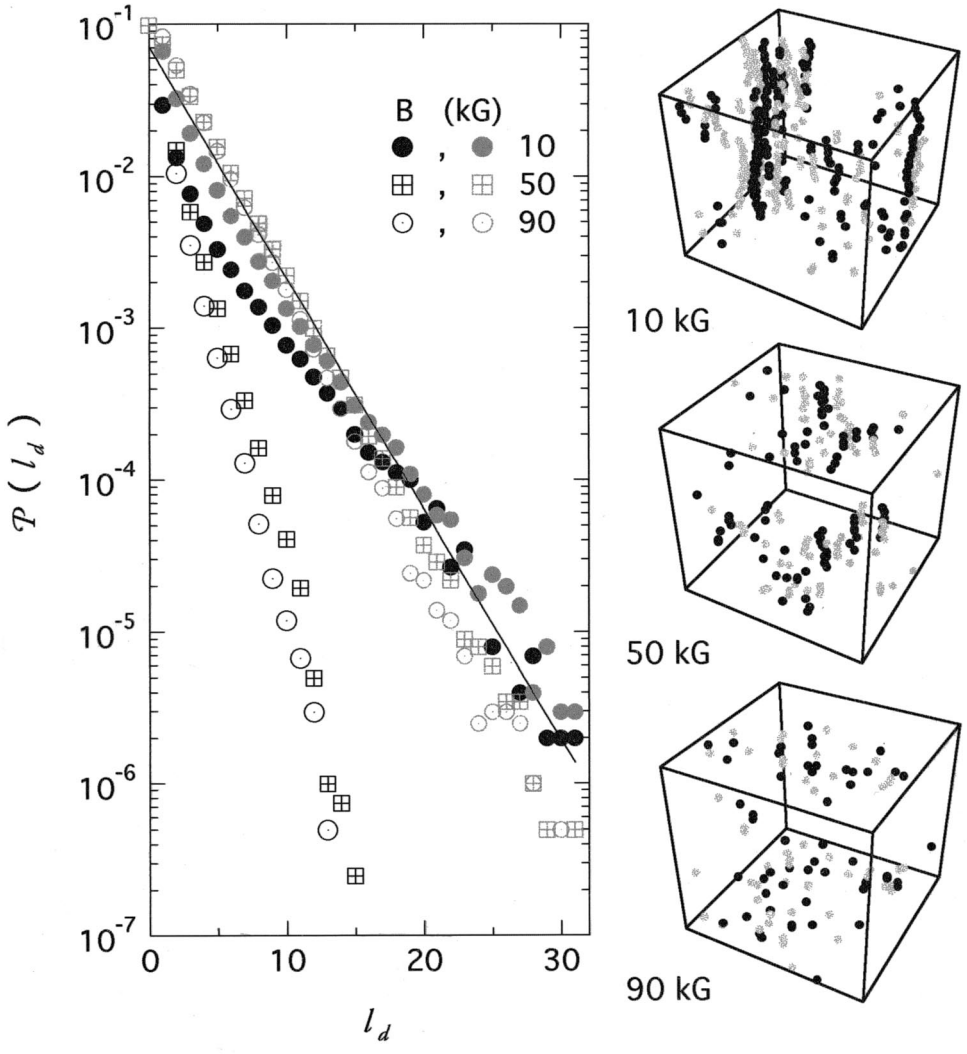

FIG. 5. Darker symbols: probability distribution of disclinations of length l_d at $B=10$, 50, and 90 kG for a 32-layer system, at temperatures such that $\delta R(B,T)=0.15$, i.e., slightly below melting. Lighter symbols: corresponding probability distributions for the same fields and system at temperatures deep into the liquid phase. In the right column, snapshots of typical defect configurations in the solid phase are shown for each field. Black and gray represent disclinations of either sign.

much shorter and occur at somewhat lower values of T/T_m. (The latter fluctuations set in at a lower temperatures because they are short and cost less energy to create.) Also shown in gray are the defect length distributions for three temperatures above the melting line, namely, $T/T_m=1.01$, 1.04, and 1.06 for $B=10$, 50, and 90 kG, respectively. In this case there is no 3D-2D crossover: The defect length distributions in these line liquid states are similar for all three fields, following a simple exponential form. [However, at the still higher temperatures $T/T_m \gtrsim 1.05, 1.07, 1.13$ respectively (not shown), $l_T > 0.2$ and the lines begin to break up into pancakes, as cutting and reconnections set in (see Sec. III D).]

To account qualitatively for these results, we note that the defects shown in Fig. 5 are line segments of isolated disclinations of various lengths. The energy E_c to create an isolated ''pancake'' (i.e., 2D) disclination defect, as is well known, is proportional to the logarithm of the system area. It may be written approximately as $E_c \approx J \ln(L^2/a_B^2)$, where L is the system edge, a_B is the lattice constant of the 2D lattice, and J is some appropriate energy, which is of the order of the intervortex interaction energy. The energy to create a line of ℓ such disclinations is therefore (neglecting momentarily the interactions between the individual pancakes) of the order of $E(\ell) \approx \ell E_c$. Since the total number of such defects in thermal equilibrium should be proportional to $\exp[-E(\ell)/k_B T]$, this argument will give the kind of exponential distribution seen numerically in both the solid and liquid phases.

To further refine this argument, we first note that $1/a_B^2$ is proportional to the magnetic induction B. Hence, for a given area and fixed J, the energy to create a 2D disclination increases as $\ln B$, which implies that the slope of the exponential dependence should become *steeper* as B increases. This increase is indeed observed in the solid phase, but it seems to be much more abrupt than the gradual increase suggested by this argument. Presumably, the abruptness stems from interactions between the disclination pancakes. If this interaction energy increases exactly as ℓ, the exponential form would be unaltered. Our numerical results show some deviation from strictly exponential behavior at low fields, suggesting that the interaction energy is more complicated. We specu-

late that this interaction energy is stronger at low fields but is reduced at larger fields, possibly by screening from other disclinations, leading to the rather sudden transition to short defects seen at high fields. But a quantitative theory of this transition remains to be developed.

Why is there no such transition in the liquid state? A possible but speculative explanation is that, in the liquid, there are many disclinations (of the order of 0.5 per plaquette per layer of the vortex lattice). Hence, they strongly screen one another, and the effective sample area L^2 in the expression for the creation energy should be replaced by the area of a plaquette, which is of order a_B^2. Then the energy to create a line of ℓ disclinations is independent of field (except possibly through the prefactor J), implying a field-independent distribution, as observed numerically.

Although the above arguments are certainly speculative, the principal numerical result, namely, a rather sharp ''3D-2D'' crossover in the defect structure, may have an experimental analog. Obara *et al.*[32] have recently reported a crossover in multilayers of $DyBa_2Cu_3O_7/(Y_{1-x}Pr_x)Ba_2Cu_3O_7$, in which a 3D vortex lattice showed only 2D correlations above ~ 10 kG. In the experimental sample, of course, the vortex lattice is affected by point pins, possibly producing a sharper crossover than we see here. Nonetheless, these pins should affect the vortex lattice quite differently at low and high fields, because the defect lines are clearly much less rigid at high fields.[33] Specifically, because of this low rigidity [as shown in $\mathcal{P}(l_d)$], the point pins may cause the defect lines to break into short segments rather abruptly at a well-defined magnetic field which may be speculatively identified with the transition observed by Ref. 32.

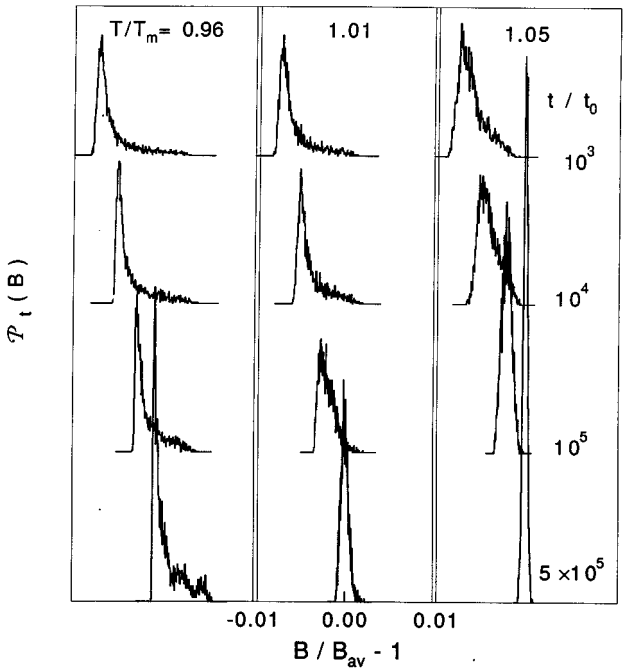

FIG. 6. Dependence of time-averaged magnetic field distribution $\mathcal{P}_t(B)$ on time window t/t_0 used for average, at an applied field of 50 kG. The time evolution is calculated at several temperatures from Langevin dynamics using Clem's prescription for computing the magnetic field (Ref. 37). The distribution is plotted as a function of $B/B_{\rm av}-1$, where $B_{\rm av}$ is the space-averaged magnetic induction. Successive distributions in each vertical panel are displaced horizontally by 0.02 units.

C. Distribution of magnetic induction in solid and liquids

Both the static and dynamic magnetic field distributions are often probed experimentally,[7,34–36] using techniques such as μSR and NMR. To calculate this distribution, we have evaluated the instantaneous local magnetic field $B(\mathbf{r},t)$ at a given time t (either by MC or LD simulation), using Clem's prescription[37] for the field of a stack of vortex pancakes. In the present case, we have an additional complication due to the periodic boundary conditions. This difficulty is again solved by including the effects of image pancakes both within the plane and along the c axis.

To obtain the dynamic evolution of the field distribution, using LD simulation, we consider the *instantaneous distribution function*

$$\mathcal{P}(B,t)=\frac{1}{V}\int dV\,\delta(B(\mathbf{r},t)-B), \tag{17}$$

which will in general depend on time, as the system approaches equilibrium. For a measurement which probes the local field averaged over a time t, we obtain the field distribution function $\mathcal{P}_t(B)$ from the following definition:

$$\mathcal{P}_t(B)=\frac{1}{V}\int dV\,\delta(\langle B(\mathbf{r},t')\rangle_t-B), \tag{18}$$

where $\langle\cdots\rangle_t$ denotes an average over a time t (either over real time, for a LD simulation, or Monte Carlo time). From the limit $t\to\infty$, we obtain the static field distribution function appropriate for μSR (in a typical μSR, the muons sample the B field at random points in a sample averaged over a typical muon lifetime of $\sim 10^{-6}$ sec) using either MC or LD simulation. A similar technique has been recently applied to obtain the static field distribution in $Bi_2Sr_2CaCu_2O_8$ using MC simulation.[38] By varying the duration t over which the local field is accumulated, we also find out how rapidly the field distribution approaches the static limit.

Figure 6 shows $\mathcal{P}_t(B)$ as calculated using LD simulation for t/t_0 ranging from 10^3 to 5×10^5 and three different temperatures above and below melting. In the long-time limit, the solid phase exhibits the characteristically asymmetric profile arising from the static triangular lattice. In the liquid, the profile becomes nearly symmetric (and very narrow) because vortices move around, producing the same time-averaged field everywhere. The distribution in the solid phase is qualitatively similar to that detected by μSR experiments in $Bi_{2.15}Sr_{1.85}CaCu_2O_{8+\delta}$.[7] Our symmetric result in the liquid appears to disagree with the experiment. The discrepancy may result from the fact that our simulation sample, in contrast to the experimental one, lacks a boundary. The possible influence of such boundaries on the field distribution observed by μSR experiments has been noted and discussed by Schneider *et al.*[38] For short-time scales ($t/t_0<10^4$), our distribution retains significant asymmetry even in the liquid phase, suggesting that the time scale for field relaxation is of this order in the liquid.

Figure 7 shows the change in rms width of the field distribution across the melting point. In the long-time limit, the

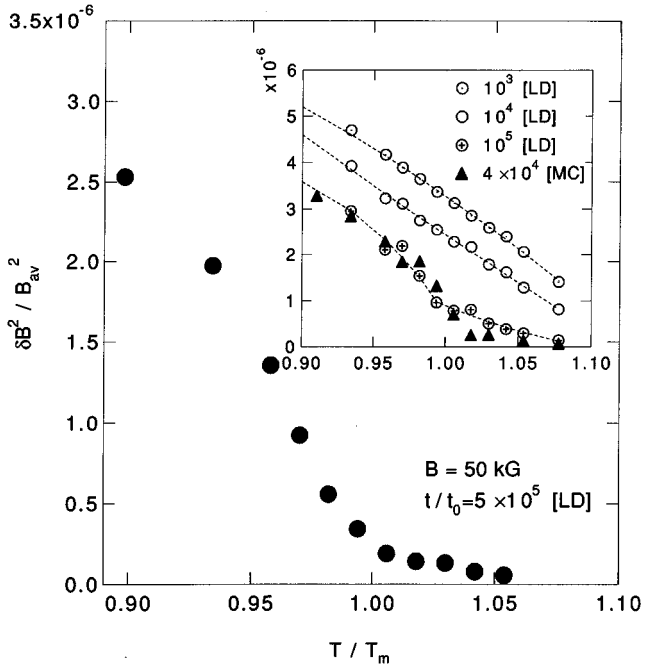

FIG. 7. Mean-square width $(\delta B)^2/B_{\rm av}^2$ of the magnetic field distribution $\mathcal{P}(B/B_{\rm av})$, plotted as a function of $T/T_m(B)$ at an applied field $B=50$ kG. The width is calculated from Langevin dynamics for time intervals of varying durations: $t/t_0=10^3$, 10^4, 10^5 (inset), and 5×10^5 (main figure). Also shown in the inset is the mean-square width as obtained from a MC simulation sampled over 4×10^4 MC steps.

temperature dependence of the width as obtained from both MC and LD simulations agrees qualitatively with NMR linewidth measurements across melting.[34] This agreement suggests that the time scale of the NMR measurement is longer than $(10^4-10^5)t_0$. Since the NMR experiments are carried out using ac fields of frequency $\sim$ MHz, this implies $10^4 t_0 \ll 1$ μsec or $t_0 \ll 10^{-10}$ sec. (This agrees with another estimate of t_0 given below.) Note also that our interpretation of NMR linewidth neglects the possibility that the ac NMR field actually exerts a force on the vortex lattice.

Two more pieces of information may be extracted from these results. First, the inset in the Fig. 7 shows that a MC result taken over 4×10^4 MC steps gives a rms width closely matching the LD result obtained with $t/t_0=10^5$. This suggests that a single MC time step using our version of the Metropolis algorithm with individual step size $\Delta x=a_B/32$ is equivalent to $\approx 2.5t_0$ of LD time. Also, from the LD results with variable t/t_0, we can infer that melting has a pronounced effect on the field distribution only when the measurement is made on time scales longer than $\sim 10^5 t_0$. In fact, the required time scale to distinguish solid from liquid may be somewhat longer than even this value in the thermodynamic limit. For the LD cell size used in these magnetic field calculations, the individual pancakes may have $\delta R(t)\propto t^\alpha$ with $\alpha\sim 1/3$ rather than $\alpha\sim 1/4$ as expected for very long lines (see below). Thus, for these thicker samples, we expect that the relevant time scale for field relaxation should be closer to $(10^5)^{4/3}t_0\sim 0.5$ μsec.

D. Relevance of vortex line cutting and reconnection

Before turning to further dynamical results, we first consider the validity of neglecting vortex line cutting and reconnection. In an earlier numerical study of $Bi_2Sr_2CaCu_2O_8$ using a similar model,[11] it was found that including line-breaking effects had little effect on the calculated melting properties. In simulations of $YBa_2Cu_3O_{7-\delta}$, which has far stiffer lines, it is reasonable to expect that the approximation is even sounder. Indeed, even in the liquid phase up to $T/T_{c2}(B)\sim 0.97$, our numerical results show that the transverse ''wandering length'' l_T, measured in units of the intervortex separation, is no larger than 0.2.

To check this approximation another way, define a ''vortex collision length'' ζ_z by $l_T^2(\zeta_z/d)^\delta\sim 1$. Presumably $\delta=1$ in the dilute (low-field) limit, where the transverse wandering of a line directed along the c axis is a random walk with step size l_T. Using 0.2 for l_T, we obtain $\zeta_z/d\sim 25$, which exceeds the thickness of our sample. In the dense regime, δ may be smaller than 1 because of the restrictive effects of the repulsive interactions among flux lines, leading to an even larger ζ_z/d.

Cutting and reconnection should occur massively only when the collision length becomes comparable to the interlayer spacing, leading to frequent ''collisions'' of vortex lines. By balancing the entropic gain from permutations of vortex connections against the accompanying cost in interlayer coupling energy, we estimate that this condition should be met only when $l_T>0.7$, which occurs only well above melting. To verify this, we did two MC runs, in one of which we allowed cutting and reconnection according to a Boltzmann weight factor obtained from the change in interlayer coupling energy that would be produced upon cutting and reconnection. The result shows that this cutting occurs at a negligible rate until $T/T_m>1.05$, at which point about 12% of recombination attempts are accepted. l_T at this temperature was found to be about 0.16, a value which may roughly be taken as a kind of ''Lindemann melting criterion'' for flux cutting in the liquid state. Thus, over much of the liquid regime, we conclude that the thermodynamics of this model can be treated without considering flux line breaking and reconnection. This conclusion justifies our treatment of flux line dynamics in the same approximation.

E. Langevin dynamics of vortex line liquids and solids: Slow and fast relaxation

Having justified our nonbreaking assumption, we return to the dynamics of vortex line liquids and solids. We begin by considering the motion of a *single* vortex line within the overdamped dynamics of Eq. (6). In the limit of a very long line in which each pancake is subject only to thermal Langevin noise and a harmonic interlayer restoring force, Eq. (6) can be solved analytically. The derivation is similar to that of Ref. 5 for more general cases. The result for the mean-square displacement of a pancake from its initial position at time t is

$$\langle|\mathbf{r}_{i,k}(t)-\mathbf{r}_{i,k}(0)|^2\rangle \approx k_B T\left(\frac{t}{d^2\eta\epsilon_d}\right)^{1/2}\int_{-\infty}^{\infty}dk\left(\frac{1-e^{-k^2}}{k^2}\right) \propto t^{1/2}, \tag{19}$$

which predicts a *sublinear* time dependence.[39] By contrast,

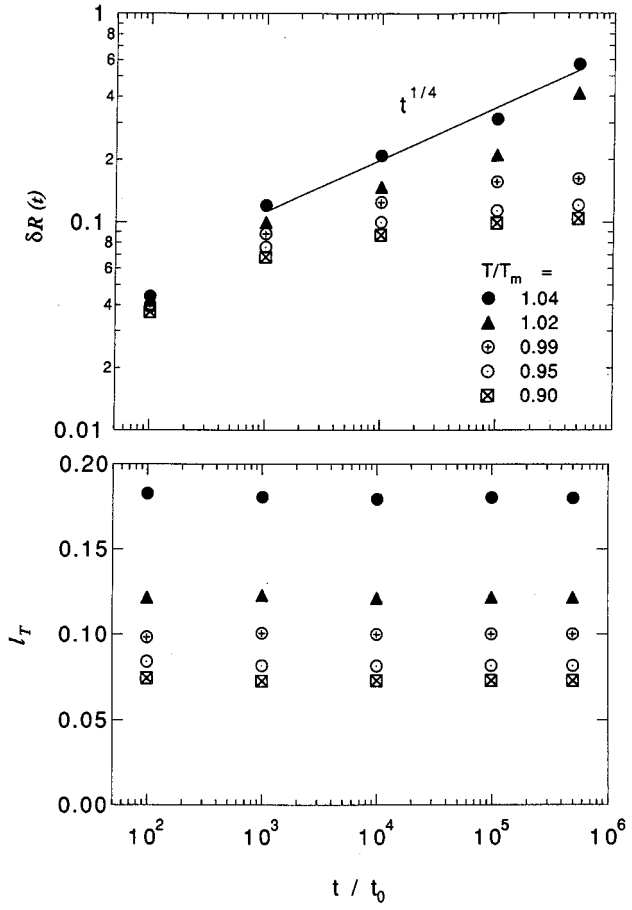

FIG. 8. (a) rms transverse displacement $\delta R(t)$ of vortex pancakes at several temperatures both above and below the melting temperature T_m, as calculated by Langevin dynamics at $B=50$ kG for $N_z=16$, and plotted in units of a_B, the mean vortex separation. For $T<T_m$, the rms displacement saturates at a value approaching the Lindemann number $c_L\approx 0.18$ at T_m. In the liquid regime, the displacement increases roughly as $t^{1/4}$, as expected for a long line, and not as $t^{1/2}$ as expected of diffusing particles. (b) Root-mean-square ''wandering length'' l_T at the same temperatures. Note that l_T saturates even in the liquid state, though its value continues to increase, primarily because of the reduction of line tension with increasing temperature.

an uncoupled pancake vortex has an ordinary diffusive transverse motion, in which $\langle|\mathbf{r}_{i,k}(t)-\mathbf{r}_{i,k}(0)|^2\rangle\propto t$.

To test this behavior, we have examined the long-time behavior of the quantity $\delta R(t)$ defined in Eq. (11) from LD simulation in the limits of (i) a single pancake vortex, (ii) a single long line, (iii) single short line segments, and (iv) an ensemble of 64 lines in 8 and 16 layers, at various temperatures both below and above T_m. For the single pancake, we observe ordinary diffusive behavior. From the limit $t/t_0\rightarrow 10^{12}$, we deduce $\mathcal{D}=1.4\times 10^{-3}$ cm^2/sec for $T=60$ K (using $t_0=1.2\times 10^{-15}$ sec; see below). This diffusion constant seems to agree reasonably well with experimental estimates for an extremely anisotropic system such as $BiSr_2Ca_2Cu_2O_8$.[40] A single line of up to 1000 vortices shows $\delta R(t)\propto t^{1/4}$ as predicted analytically, while lines shorter than $4d$ show behaviors close to a 2D diffusion.

Figure 8 shows case (iv) for $B=50$ kG and 16 layers of $YBa_2Cu_3O_{7-\delta}$ at five temperatures above and below T_m. For $T<T_m$, vortex excursions are limited to radii smaller than the appropriate Lindemann distance of around $0.2a_B$. For $T>T_m$, the rms displacement seems to grow with an approximately $t^{1/4}$ behavior as expected from the analytic estimate for a single line. In the case of an eight-layer system (not shown), we observed $\delta R(t)\propto t^{1/3}$, possibly indicating that the system lies between the long-line and 2D limits. In both cases, the motion of individual pancakes is slower than in the usual Brownian diffusion. Hence, in the long-time limit, a diffusion constant defined on the assumption of a linear t dependence will vanish even in the liquid regime and even without pinning. At sufficiently high temperatures, of course, line cutting will eventually set in (though not in the present approximate model). With line cutting, the system may then cross over to a 2D liquid with ordinary diffusive behavior. Therefore, there is an interesting possibility of two different types of liquids characterized by different diffusive behavior, with a smooth crossover between them.

As a further means of studying relaxation in the solid and liquid phases, we have monitored the LD evolution of various thermodynamic quantities, such as various components of internal energy and the defect density, after the system is initialized in some arbitrary nonequilibrium state. For each temperature, we considered five different initial states. Each initial state was prepared by randomly and rigidly displacing the individual vortex lines from a perfect triangular lattice by an amount not exceeding a fraction α_r of the mean intervortex spacing. In most cases, a rapid exponential relaxation of energy is observed. By fitting the time-dependent internal energy to the form $a+b\exp[-t/\tau_r]$, we find a relaxation time τ_r which increases with increasing temperature (cf. Fig. 9, for which $\alpha_r=0.31$). This increase is once again due mainly to an energy scale which diminishes [or a $\lambda_{ab}(T,B)$ which increases] with increasing T.

Superimposed on this overall trend, there may be a peak in τ_r corresponding to enhanced fluctuations precisely at the melting temperature (although there are large uncertainties at this temperature). This behavior is consistent with expectations for a phase transition with a kinetic or ''critical'' slowing down, but the feature is generally concealed by the steep increase of τ_r with increasing temperatures, and can hardly be used to distinguish between possible first-order and continuous phase transitions. The middle row of Fig. 9 shows the progression of the density correlation function from an initial random configuration to a well-ordered state over a period of about $100t_0$ at a temperature $T/T_m=0.9$. The lower row shows the local instantaneous magnetic field profile for the initial and final configurations in a particular layer. The cores of the vortices lie at the centers of the bright regions.

In Fig. 10, we show a typical relaxation of total internal energy over time after an initial randomization, this time with $\alpha_r=0.63$. Also shown is the density of isolated disclinations, n_d^*. In contrast to the internal energy, which relaxes exponentially, the disclination density relaxes toward zero (i.e., an elastic lattice) with a roughly ln$t$ behavior. The disclinations finally disappear (via pair annihilation) long after the internal energy has nearly equilibrated. The spikes in n_d^* on top of the overall logarithmic decay may correspond to a large-scale rearrangements of vortices, possibly involving activated processes. The energy relaxation itself shows no obvious signature of any such activated processes.

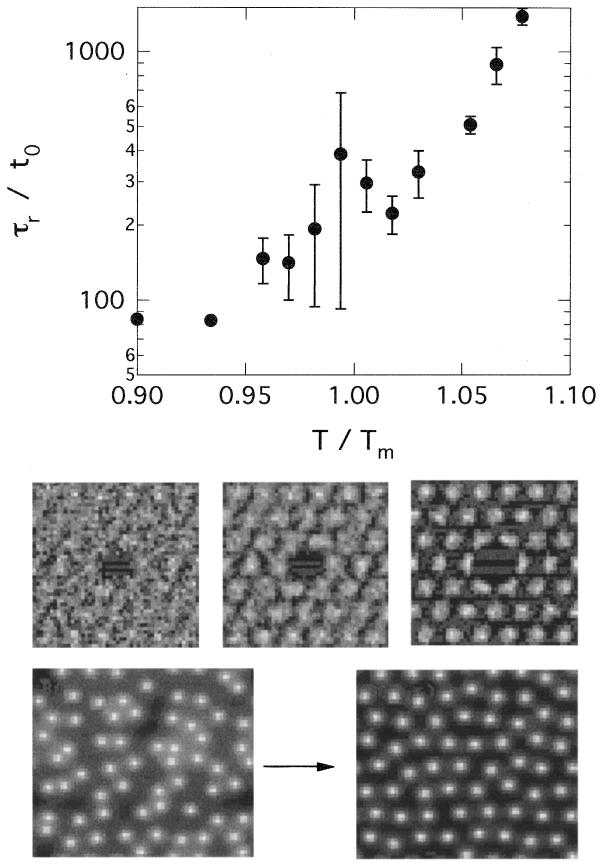

FIG. 9. Top: relaxation time τ_r describing return of vortex system to its equilibrium configuration, following an initial perturbation, as plotted for several temperatures in the flux solid and flux liquid state. Calculation is carried out as described in the text. Error bars are standard deviations from five different initial configurations. Middle: snapshots of density-density correlation function $C(\mathbf{r},z=0)$ for three representative configurations during relaxation at $T/T_m=0.89$. Bottom: evolution of local field $B(\mathbf{r},t)$ in a specific ab plane of the sample, for the first and third configurations of middle panel.

To understand real materials, we next examine how point pins influence these general features. In Fig. 11, we show the relaxation of the in-plane component of the internal energy for different pinning strengths ($0<\alpha_p<5$) with an areal density equivalent to $B_p=888$ kG. The relaxation is qualitatively different from the weak-pinning cases ($\alpha_p\leqslant 3$), in which the energy typically decays exponentially as in clean systems. At $\alpha_p=5$, for example, the in-plane part of the energy varies logarithmically with time almost from $t=0$.

For pins of any strength, we find that the system never relaxes back to the perfect triangular lattice within our simulation times; a significant fraction of disclinations always survives even after $t/t_0=5\times10^5$ (cf. lower part of Fig. 12). Possibly, early-stage relaxation is controlled mainly by pinning forces. But once the pinning energy is nearly optimized by this quick relaxation, all driving forces for relaxation become comparable in strength (after $t/t_0\approx3\times10^4$), and relaxation slows dramatically. Any further relaxation must reduce the elastic strain energy without sacrificing pinning energy. To accomplish this, both total and isolated defect densities slowly but steadily decrease (with many fluctuations). Also,

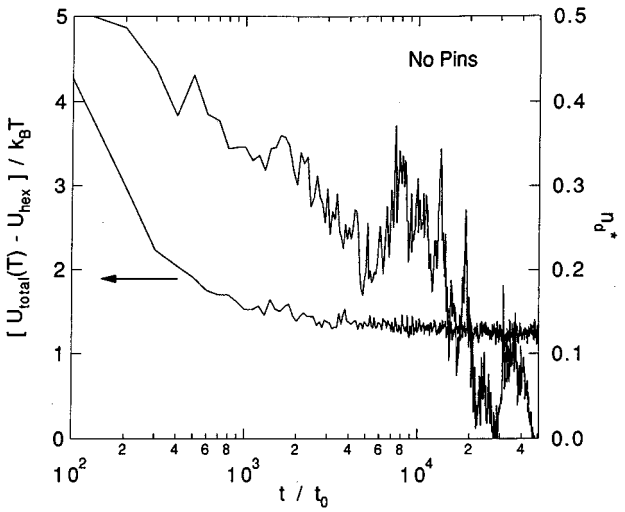

FIG. 10. Time dependence of total internal energy $U_{\text{total}}(T)$ per pancake (left-hand scale) and the isolated disclination density n_d^* (right-hand scale), as calculated via LD simulation at $B=50$ kG, $T/T_m=0.898$, starting from a randomized initial configuration in a pin-free sample. U_{hex} is the internal energy of an ideal hexagonal lattice at the same temperature.

n_d^*/n_d (lower panel of figure) decreases noticeably for $t/t_0>3\times10^4$. In other words, energy relaxation in this regime is proceeding via a decrease in the number of isolated defect configurations.

The slow elastic relaxation just described must involve vortex rearrangement. It may therefore affect measurements of the local magnetic field and the total magnetization. Indeed, such quantities have long been known to depend

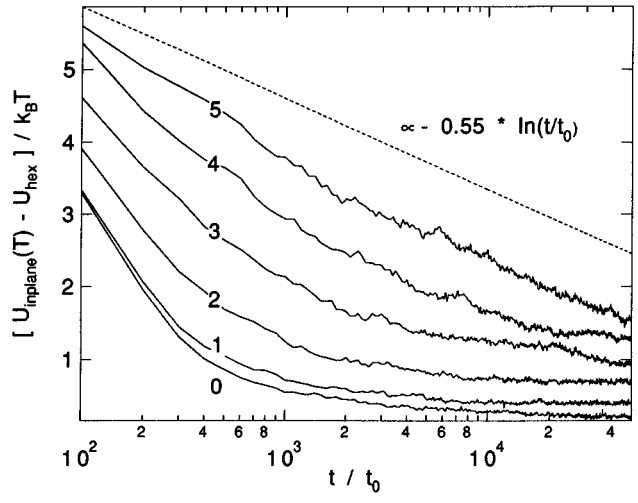

FIG. 11. Relaxation of in-plane portion of internal energy per pancake, $U_{\text{in-plane}}$, for point pins of varying strength ($0\leqslant\alpha_p\leqslant5$). The initial configuration is a randomized distribution of straight vortex lines with $\alpha_r=0.63$ (see text). Note the gradual crossover from an exponential to a logarithmic time dependence as the pinning strength increases. At the largest value of α_p, the relaxation is dominated by changes in the pinning energy. Other conditions same as in the previous figure. U_{hex} is here the in-plane part of the internal energy of an ideal hexagonal lattice (per pancake) at the same temperature.

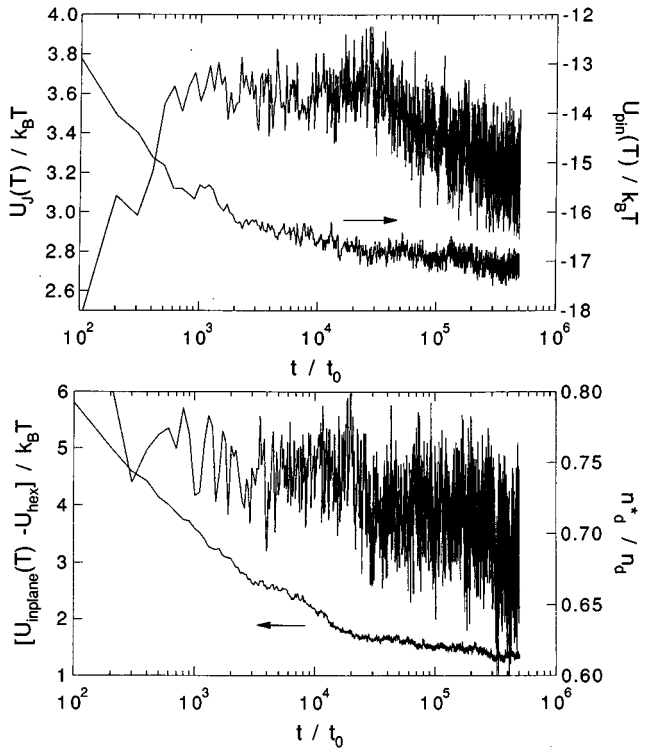

FIG. 12. Time dependence of interlayer part of internal energy $U_J(T)$, pinning energy $U_{\rm pin}(T)$, in-plane component of elastic energy $U_{\text{in-plane}}(T)$, and ratio of isolated disclination density n_d^* to total disclination density n_d, for strong pinning ($\alpha_p=5$), at a temperature of $T/T_m=0.898$ where T_m is the melting temperature for a pin-free sample.

strongly on the time scale over which they are measured. Thus, our model can help to explain such slow relaxation of magnetization, in disordered samples. The calculations also suggest that the slow relaxation results predominantly from the rearrangement and annealing-out of topological defects.

Next, we briefly discuss the value of t_0, which is crucial in connecting our numerical results to experiments on real materials. The friction coefficient η is related to the flux-flow resistivity $\rho_{\rm ff}$ by the equation $\rho_{\rm ff}=B\phi_0/\eta c^2$. Assuming a flux-flow resistivity $\rho_{\rm ff}$ ($B=50$ kG, $T/T_m=0.9)\sim 0.16\rho_n$, where ρ_n is the normal-state resistivity, and estimating ρ_n as its value at $T_c(0)$, $\rho_n(T_c(0))\sim 100\ \mu\Omega$ cm (Ref. 41) for a single crystal of $YBa_2Cu_3O_{7-\delta}$, we obtain $\rho_{\rm ff}\approx 1.6\times 10^{-17}$ sec. The corresponding value of t_0, assuming the time step in Sec. II C, is $t_0\approx 10^{-14}$–10^{-15} sec. Since our value of $\rho_{\rm ff}$ is probably an overestimate, this value should be taken as the lower bound for t_0.[42]

Finally, we briefly return to the influence of pins on the dynamics of flux lines, in light of this value for t_0. In real materials, such pins will strongly affect flux line dynamics, typically slowing down their motion by several orders of magnitudes (as we have noted above). This has some implications for interpreting the experimental results which are sensitive to the time evolution of local magnetic field. One such experiment is the spin-echo NMR probe[40,43] in the highly anisotropic Tl-based compounds. This has been interpreted as implying a vortex diffusion constant $\mathcal{D}$ of $10^{-4}\sim 10^{-5}$ cm^2/sec at temperatures $T\lesssim T_m$, and of $\approx 10^{-3}$–10^{-4} cm^2/sec for $T>T_m$. On the other hand, more recent spin-echo results on aligned powders of $YBa_2Cu_3O_{7-\delta}$ seem to show lack of diffusion even on very long time scale.[35,36] These results may indicate the presence of strong pins in the powder samples, which greatly slow down the dynamics. Another possibility is that the discrepancy is somehow due to the nondiffusive behavior of long lines discussed above.

IV. DISCUSSION AND CONCLUSIONS.

We have presented a detailed numerical study of the vortex structure in a model for $YBa_2Cu_3O_{7-\delta}$, both above and below the flux lattice melting temperature, using Monte Carlo and Langevin simulations. Our results indicate that in clean $YBa_2Cu_3O_{7-\delta}$, there is a weakly first-order melting transition, with a very small heat of fusion which agrees the calculations of Ref. 3 at similar fields.

We also find that there is a striking change in distribution of local magnetic fields at melting: The time-averaged magnetic field sensed by a fixed particle in the sample has a very narrow distribution in the liquid (because the vortices move around in the liquid), but acquires an asymmetric distribution of finite and temperature-dependent width in the solid phase. This behavior agrees with both μSR and NMR experiments in $YBa_2Cu_3O_{7-\delta}$. Although some previous MC calculations[38] have suggested a similar transition, our LD simulations provide more information. In particular, because the time constant of the Langevin simulations can be extracted from measurements of the liquid-state resistivity, we can estimate the measurement time necessary to distinguish the solid and liquid field distributions. This time appears to be about 0.5 μsec in $YBa_2Cu_3O_{7-\delta}$ at a field of 50 kG.

Our calculations show that there is a qualitative change in the structure of the topological defects in the crystalline phase just below melting. Namely, even in clean $YBa_2Cu_3O_{7-\delta}$, there are long lines of disclinations parallel to the c axis at relatively low fields ($B\lesssim 10$ kG), but these break up into short (''2D'') disclinations at higher fields. We believe that this breakup may be an essential ingredient in the ''3D-2D'' transition recently reported in Bi-Sr-Ca-Cu-O.[6,32,33] In clean systems, we find numerically that the distribution of defect line lengths is approximately exponential in the liquid, but deviates from exponential in the solid phase. We account for these forms by a simple model of topological defects in the vortex lattice of a layered superconductor.

A remarkable result of our Langevin simulations is that the vortex lines move nondiffusively even in the liquid state — that is, the rms displacements of the vortex pancakes vary like t^α, where $\alpha<0.5$. This agrees with the exact result derived for a single long line,[39] that the rms displacement of a sufficiently long vortex line subject to thermal noise varies as $t^{1/4}$. Our simulations suggest that the behavior is also found in a dense line liquid with strong short-range repulsive interactions. While the full transport implications remain to be explored, this result is consistent with recent NMR measurements on $YBa_2Cu_3O_{7-\delta}$,[36] which also suggest that in the liquid state vortex lines move subdiffusively.

The LD calculations also reveal that the vortices relax much more slowly as $T\to T_{c2}(B)$. Such slow relaxation is actually built into the TDGL equation, whose time constant

is proportional to the deviation of the Ginzburg-Landau free energy from its minimum value. Since the minimum becomes ever shallower as $T_{c2}(B)$ is approached, the relaxation time constant should become ever longer. It would be most interesting to have experimental confirmation of this behavior. The Langevin results also suggest that the time constant may increase as the (first-order) melting transition is approached from either side.

A final conclusion has to do with the influence of point pins on the dynamics. Our Langevin results show that, after any disturbance, the energy relaxes nearly exponentially back to equilibrium in a pin-free sample. With strong pins present, however, the energy relaxation is close to logarithmic in time. At even longer time scales, there is a crossover to a logarithmic relaxation with a different slope. We identify this slower relaxation with the logarithmically slow annealing-out of topological defects in the disordered samples (these same defects are also slow to disappear in the pin-free case). It has long been known that many properties of the high-T_c materials vary logarithmically slowly with time (most notably, the sample magnetization). Our model, which treats in a fairly realistic manner a disordered $YBa_2Cu_3O_{7-\delta}$ sample, clearly produces such slow relaxation, and identifies it with a particular type of topological defect dynamics.

In summary, we have presented a detailed study of the nature of the flux line melting based on the vortex representation of the Lawrence-Doniach model, using both Monte Carlo and Langevin simulations in a consistent way. We calculate a wide range of properties of both the vortex solid and liquid phases which are consistent with experiment, and which shed light on the topological defects which underlie the melting process, as well as the time-dependent magnetization and magnetic field distribution, of these materials.

ACKNOWLEDGMENTS

We are grateful for valuable discussions with Professor C. H. Pennington and C. Recchia. This work was supported by DOE Grant No. DE-FG02-90 ER45427 through the Midwest Superconductivity Consortium at Purdue University, by NSF No. Grant DMR94-02131. D.S. thanks the Department of Applied Physics at Stanford University and Professor S. Doniach for their kind hospitality during the completion of this work. Calculations were carried out, in part, with the use of the computational facilities of the Ohio Supercomputer Center.

*Electronic address: ryu@pacific.mps.ohio-state.edu
†Permanent address.

[1] M. Franz and S. Teitel, Phys. Rev. Lett. **73**, 480 (1994).
[2] Z. Tešanović and L. Xing, Phys. Rev. Lett. **67**, 2729 (1991); J. Hu, Ph.D. dissertation, Indiana University, 1994; J. Hu and A. H. MacDonald, Phys. Rev. Lett. **71**, 432 (1993); Y. Kato and N. Nagaosa, Phys. Rev. B **48**, 7383 (1993).
[3] R. Šášik and D. Stroud, Phys. Rev. Lett. **75**, 2582 (1995).
[4] E. Brézin, D. R. Nelson, and A. Thiaville, Phys. Rev. B **31**, 7124 (1985).
[5] G. Blatter, M. V. Feigel'man, V. B. Geshkenbein, A. I. Larkin, and V. M. Vinokur, Rev. Mod. Phys. **66**, 1125 (1995).
[6] R. Cubitt, E. M. Forgan, G. Yang, S. L. Lee, D. M. Paul, H. A. Mook, M. Yethiraj, P. H. Kes, T. W. Li, A. A. Menovsky, Z. Tarnawski, and K. Mortensen, Nature **365**, 407 (1993).
[7] S. L. Lee *et al.*, Phys. Rev. Lett. **71**, 3862 (1993).
[8] H. Safar *et al.*, Phys. Rev. Lett. **69**, 824 (1992).
[9] E. Zeldov, D. Majer, M. Konczykowski, V. B. Geshkenbein, V. M. Vinokur, and H. Shtrikman, Nature **375**, 373 (1995).
[10] L. Xing and Z. Tešanović, Phys. Rev. Lett. **65**, 794 (1990).
[11] S. Ryu, S. Doniach, G. Deutscher, and A. Kapitulnik, Phys. Rev. Lett. **68**, 710 (1992).
[12] (a) Y. Enomoto and K. Katsumi, Phys. Lett. A **169**, 287 (1992); (b) Y. Enomoto, *ibid.* **176**, 153 (1993); (c) Y. Enomoto, K. Katsumi, and S. Maekawa, Physica C **215**, 51 (1993); (d) Y. Enomoto and S. Maekawa, *ibid.* **233**, 195 (1994).
[13] W. R. Magro and D. M. Ceperley, Phys. Rev. B **48**, 411 (1993).
[14] D. Reefman and H. B. Brom, Physica C **213**, 229 (1993).
[15] M. I. J. Probert and A. I. M. Rae, Phys. Rev. Lett. **75**, 1835 (1995).
[16] Y.-H. Li and S. Teitel, Phys. Rev. Lett. **66**, 3301 (1991).
[17] R. E. Hetzel, A. Sudbø, and D. A. Huse, Phys. Rev. Lett. **69**, 518 (1992).
[18] W. Y. Shih *et al.*, Phys. Rev. B **30**, 134 (1984).
[19] M. P. A. Fisher, Phys. Rev. Lett. **62**, 1415 (1989).
[20] D. R. Nelson and V. M. Vinokur, Phys. Rev. Lett. **68**, 2398 (1992).
[21] For an example of related *gauge glass* model, see J. D. Reger, T. A. Tokuyasu, A. P. Young, and M. P. A. Fisher, Phys. Rev. B **44**, 7147 (1991).
[22] For example, see K. H. Lee, D. Stroud, and S. M. Girvin, Phys. Rev. B **48**, 1233 (1993), and references therein.
[23] The choice of temperature dependence is based on the measurements of D. R. Harshman *et al.*, Phys. Rev. B **36**, 2386 (1987). The field dependence is taken from M. Tinkham, *Introduction to Superconductivity* (McGraw-Hill, New York, 1975), p. 125.
[24] W. E. Lawrence and S. Doniach, in *Proceedings of LT12*, Kyoto, 1970, edited by E. Kanda (Keigaku, Tokyo, 1971).
[25] J. P. Carton, J. Phys. (France) I **1**, 113 (1991).
[26] J. R. Clem and M. W. Coffey, Phys. Rev. B **42**, 6209 (1990).
[27] M. V. Feigel'man, V. B. Geshkenbein, and A. I. Larkin, Physica C **167**, 177 (1990).
[28] S. Doniach, in *High Temperature Superconductivity*, Los Alamos Symposium, edited by K. S. Bedell, D. Coffey, D. E. Meltzer, D. Pines, and J. R. Schrieffer (Addison-Wesley, Redwood City, CA, 1989), p. 412.
[29] To carry out the image calculation for the in-plane interaction, we use $K_0^*[|\mathbf{r}_{i,k}|/\lambda_{ab}(T,B)]=\Sigma_m K_0[(|\mathbf{r}_{i,k}+L_x m_x\hat{x}+L_y m_y\hat{y})/\lambda_{ab}(T,B)]$, where m_x and m_y are integers satisfying $m_x^2+m_y^2\leq N_m^2$, L_x and L_y are the edges of the simulation cell, and N_m is a suitably chosen upper limit to the summation. Typically we use $N_m\sim 40$, but vary the value with $\lambda_{ab}(T,B)$ to ensure optimum convergence. If the lattice sum converges insufficiently, the triangular lattice may become unstable against formation of a square lattice; this leads to a spurious structural transition in a certain temperature window. We have carefully included enough terms in our image summation to prevent this spurious transition from taking place.
[30] M. C. Hellerqvist, S. Ryu, L. W. Lombardo, and A. Kapitulnik, Physica C **230**, 170 (1994).
[31] F. P. Preparata and M. I. Shamos, *Computational Geometry*

(Springer-Verlag, New York, 1985).
[32] H. Obara *et al.*, Phys. Rev. Lett. **74**, 3041 (1995).
[33] A similar transition in disordered samples of $BiSr_2Ca_2Cu_2O_8$ has been reported in simulations by S. Ryu, A. Kapitulnik, and S. Doniach (unpublished).
[34] C. H. Recchia, C. H. Pennington, H. Hauglin, and G. P. Lafyatis, Phys. Rev. B **52**, 9746 (1995).
[35] C. Recchia and C. Pennington (unpublished).
[36] Y. Q. Song *et al.*, Phys. Rev. Lett. **75**, 2008 (1995).
[37] J. R. Clem, Phys. Rev. B **43**, 7837 (1991).
[38] J. W. Schneider, S. Schafroth, and P. F. Meier, Phys. Rev. B **52**, 3790 (1995).
[39] A more general result, for manifolds of dimension $d=1,2,3$ moving under the influence of thermal noise, has been given by Ref. 5.
[40] Y. Q. Song *et al.*, Phys. Rev. Lett. **72**, 177 (1994).
[41] X. Iye *et al.*, Physica C **153-155**, 26 (1988).
[42] This estimate is for a clean, i.e., a pin-free, system. The influence of the pins could possibly be approximated by a renormalized effective friction coefficient. But since the effect of pins varies widely from sample to sample, it may be difficult to extract a reliable value of η from experiment.
[43] J. T. Moonen *et al.*, Phys. Rev. Lett. **72**, 176 (1994).